

Graph Neural Networks Accelerated Molecular Dynamics

Zijie Li,[†] Kazem Meidani,[†] Prakarsh Yadav,[†] and Amir Barati Farimani^{*,†,‡,¶}

[†]*Department of Mechanical Engineering, Carnegie Mellon University, Pittsburgh PA, USA*

[‡]*Machine Learning Department, Carnegie Mellon University, Pittsburgh PA, USA*

[¶]*Department of Chemical Engineering, Carnegie Mellon University, Pittsburgh PA, USA*

E-mail: barati@cmu.edu

Abstract

Molecular Dynamics (MD) simulation is a powerful tool for understanding the dynamics and structure of matter. Since the resolution of MD is atomic-scale, achieving long time-scale simulations with femtosecond integration is very expensive. In each MD step, numerous redundant computations are performed which can be learnt and avoided. These redundant computations can be surrogated and modeled by a deep learning model like a Graph Neural Network (GNN). In this work, we developed a GNN Accelerated Molecular Dynamics (GAMD) model that achieves fast and accurate force predictions and generates trajectories consistent with the classical MD simulations. Our results show that GAMD can accurately predict the dynamics of two typical molecular systems, Lennard-Jones (LJ) particles and Water (LJ+Electrostatics). GAMD's learning and inference are agnostic to the scale, where it can scale to much larger systems at test time. We also performed a comprehensive benchmark test comparing our implementation of GAMD to production-level MD softwares, where we showed GAMD is competitive with them on the large-scale simulation.

1 Introduction

Molecular Dynamics (MD) is a simulation method that has been extensively used in material science, physical chemistry, and biophysics. In MD simulations, the trajectories of atoms, particles, and molecules are generated by iteratively solving Newton’s equations representing the interacting particles. To ensure the stability of the simulations with atomic-scale resolution, very short time steps in the order of femtoseconds are used for the integration. However, many of the biochemical and other systems of interest have much longer time scales of nano- or micro-seconds.¹ Therefore, achieving these long time-scale simulations is compute-intensive despite using state-of-the-art computational powers such as GPUs and acceleration techniques. Simulating large scale systems such as viruses for realistic timescales (milliseconds to seconds) is almost impossible. Another fact that makes MD simulations time-consuming is that there are huge amounts of redundant computations performed in each iteration of the simulation. These repetitive computations include the calculation of forces acting on each particle summed up from various pair, bonded or non-bonded, forces in the system. Avoiding these reiterating steps is an opportunity for algorithmic improvement to reach more efficient MD simulations.²⁻⁶

Besides iterative computations, other concerns related to MD simulations come from the accuracy of calculations and approximations required to describe complex interatomic forces between particles. There are a wide variety of types of interactions that are strongly dependent on the types of particles, their bonded or non-bonded interactions, and the environment conditions. Therefore, a detailed full-physics model is usually required to achieve a simulation with sufficient precision and consistency with the real event.

Machine learning has provided the opportunity to learn many of the complex physics-based systems from examples gathered from huge amounts of data. There have been active lines of research in various fields to learn models to simulate complex systems governed by well-known, partially-known, or even unknown physics.⁷⁻⁹ Presumably, the learned model can accelerate the simulation, prediction, or control of the systems by surrogating the full

physics model. Besides time efficiency, proposed models have to perform well in terms of both accuracy, within the training data distribution, and generalization, beyond what the model is trained on. Similar to many other fields, accelerated surrogate models have been introduced for machine learning force field in molecular simulations.^{10,11} Additional acceleration and application on larger systems can also be achieved by using the idea of learning coarse-grained force fields. Although some thermodynamic consistency can be attained by coarse-grained networks, there is a considerable information loss on more detailed structures and properties of the systems.^{12,13}

Deep neural networks have shown promising results in molecular and material property predictions, and molecular simulations.¹⁴⁻¹⁶ The classical approaches of using machine learning have mostly been feature engineering methods by finding tailored molecular representations of the system that capture essential characteristics of the complex system.^{6,17} For example, atom-centered symmetry functions (ACSFs) have been used in Behler-Parrinello Neural Networks (BPNN)¹⁸⁻²⁰ for translation- and rotation-invariant energy conservation.

Graph Neural Networks (GNNs), with convolution layers specialized for unstructured data, have recently been used to learn various physics-based models and to accelerate them.²¹⁻²⁴ In molecular systems, they have shown a performance boost as well as an end-to-end learning opportunity that bypasses the need for manual feature representations by learning the properties automatically from the atomic observations.²⁵⁻²⁸ GNNs encode information about particles, their properties, and the neighbor interactions in the nodes and edges of the defined graph. The interactions can be described in the general form of message passing neural networks (MPNNs)²⁹ where information is passed between neighbor atoms, i.e. nodes, in the graph.

Based on the output of the models, recently proposed deep neural networks for MD force field prediction have been categorized to energy-centric and force-centric models. Energy-centric models explicitly conserve the energy of the system by predicting and controlling the energy as the output or by observing forces as the negative gradient of the conserved

energy.³⁰ Force-centric models, however, directly predict and compare forces generated by the model with the ground truth forces. In fact, the network’s outputs are per-node, i.e. per-atom, forces.

To date, most of the proposed models are energy-centric, meaning that they directly conserve the system’s energy by their architecture and loss function design.^{31,32} For example, energy conservation can be described by Hamiltonian of a conservative system. Single body or many body forms of Hamiltonian have been used in different applications to apply conservation constraint while using automatic differentiation to compute the derivatives, i.e. states and forces.³³⁻³⁵

Besides, the energy surface can be directly predicted by the model, and forces can be extracted as the gradient of energy. Gradient-Domain Machine Learning (GDML) and symmetrized GDML (sGDML)^{30,36} conserve energy by learning explicit gradient function mapping of energy and interatomic forces. As another energy-centric model, SchNet³⁷ employs continuous convolution filters to learn features on graph networks for smooth energy predictions. DimeNet^{38,39} is another more complex energy-centric model that, though slower than SchNet, shows better generalization to different molecules and configurations. Several deep learning frameworks have been built based on differentiable physics to employ classical MD and machine learning potentials learned by these energy-centric models.^{2,3,40}

In another family of models, forces can be predicted directly using force-centric networks. Although force-centric models do not possess any strict energy conservation mechanism, they have shown some promising advantages. First, they do not need to consider the accumulation of several types of energy and thus are usually computationally more efficient.^{4,5,41} Moreover, they show better prediction accuracy than energy-centric models. The reason lies behind the fact that small noises, and errors, in energy predictions can be enhanced by taking derivatives to compute the forces from the energy predictions.

Force-centric models have been applied in several applications to infer the forces in fluids,⁷ glassy systems and solid-state MD simulations,^{4,5,8} as well as large-scale quantum property

calculations.⁴¹ Bypassing the calculations required for taking derivatives of potential energy surface (PES) have brought about computational efficiency in neural network force field (NNFF)⁴ and Graph NNFF (GNNFF)⁵ models. Using Density Functional Theory (DFT)-calculated forces as ground truth, GNNFF can learn atomistic level dynamics of solid-state material systems. In another study, ForceNet⁴¹ shares the common backbone of using Graph Network-based simulators (GNS) framework to predict forces by using massive physics-based augmented data rather than using any architectural constraints. These models show faster and yet accurate predictions of quantum properties and forces in comparison to benchmarks like SchNet.³⁷ Despite promising results obtained by these models, there is still need for a generalizable and scalable framework that can learn MD force fields in challenging and large scale molecular dynamics such as a water box. Also, a thorough study of applying such force-centric GNN framework to learn MD force fields in order to accelerate an entire simulation has not been performed yet. A detailed evaluation of the computational time efficiency of these models has also remained largely unexplored.

In this work, we present a Graph Accelerated Molecular Dynamics (GAMD) framework as a new force-centric model to learn various empirical force fields from molecular dynamics simulations. We show that by careful training of a rotation-covariant graph model, we can bypass the physics-based neighbor selection and energy calculation step of traditional MD simulations by direct GNN force prediction. In fact, GAMD avoids numerous iterative and redundant computations required to calculate per-atom forces in long molecular dynamics. Consequently, it brings about a significant boost of computational efficiency in the simulations. We show that GAMD can generate MD trajectories that are spatially (based on Radial Distribution Function) and temporally (based on kinetic energy and equilibrium) coherent compared to classical MD methods. Moreover, our benchmark shows that GAMD’s calculation efficiency is competitive among several production-level MD engines on large-scale simulation.

2 Methods

2.1 Molecular Representation

A molecular system at a certain state can be described as: $\mathbf{X} : (\mathbf{q}_1, \mathbf{q}_2, \dots, \mathbf{q}_n)$, where $\mathbf{q}_i, \forall i \in \{1, 2, \dots, n\}$ denotes the Cartesian coordinates of each atom in the system. Through the network, we represent atoms as nodes in a GNN and interactions between atoms as edges. Concretely, the node input features is a one-hot vector \mathbf{p}_i , which specifies the atom type. The edge input feature is a vector derived by concatenating inter-atomic distance vector \mathbf{q}_{ij} and a one-hot vector \mathbf{b}_{ij} which indicates the edge type between two atoms (i.e. whether two atoms are bonded in the same molecule). The inter-atomic distance vector is defined by concatenating the directional vector and the norm of relative position: $\mathbf{q}_{ij} = (\frac{\mathbf{q}_i - \mathbf{q}_j}{\|\mathbf{q}_i - \mathbf{q}_j\|_2}, \|\mathbf{q}_i - \mathbf{q}_j\|_2)$. With the introduction of directional vector, the edge is directed and thus $\mathbf{e}_{ij} \neq \mathbf{e}_{ji}$.

To further leverage the expressiveness of neural networks, we lift node input features \mathbf{p}_i and edge input features $(\mathbf{q}_{ij}, \mathbf{b}_{ij})$ into high-dimensional vector embedding $\mathbf{v}_i^{(0)}, \mathbf{e}_{ij}^{(0)} \in \mathbb{R}^d$ (with d being the dimension of latent space) via learnable encoders ϵ^V and ϵ^E (Figure 1, Feature Encoding), which are built upon multi-layer perceptrons (MLPs).

$$\begin{aligned}\mathbf{v}_i^{(0)} &= \epsilon^V(\mathbf{p}_i) \\ \mathbf{e}_{ij}^{(0)} &= \epsilon^E(\mathbf{q}_{ij}, \mathbf{b}_{ij})\end{aligned}\tag{1}$$

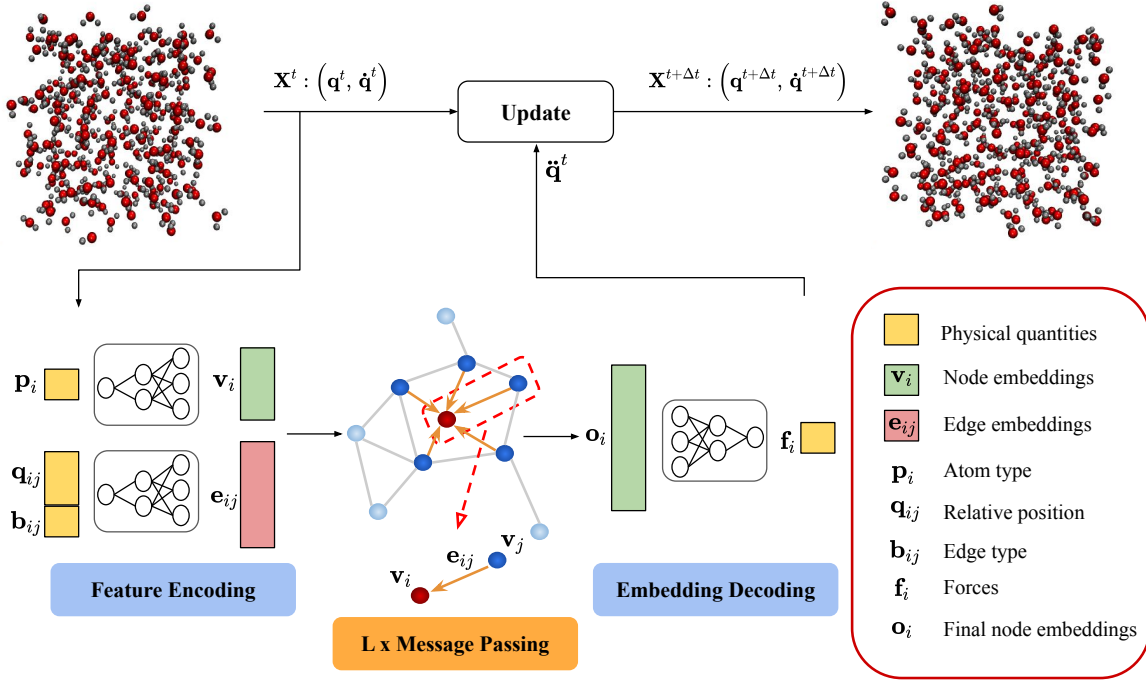


Figure 1: Overview of GAMD schematic. GAMD uses graph neural networks (GNN) to predict the forces of atoms \mathbf{f}_i in the molecular system $\forall i \in \{1, 2, \dots, n\}$ given properties of atoms \mathbf{p}_i (i.e. type of atoms), positions of atoms \mathbf{q}_i , and edge type between two atoms \mathbf{b}_{ij} . The features are first encoded using multi-layer perceptron (MLPs), and then inferred using an atom-wise message passing scheme. At last, an MLP decoder predicts forces from the node embeddings. Based on the predicted forces, GAMD forwards the dynamics of the system by imposing acceleration $\ddot{\mathbf{q}}$ on each atom.

2.2 Atom-wise Message Passing

The inference and prediction of molecular information utilizes a recurring atom-wise message passing block (Figure 1, Message Passing). Inside each block, the center atom i first collects messages from all the neighbor atoms $\forall j \in \mathcal{N}(i)$. The message $\mathbf{m}_{j \rightarrow i}^{(l)}$ is conditioned on the edge embedding $\mathbf{e}_{ij}^{(l-1)}$ which carries the inter-atomic directional information and interaction type between two particles, along with node features from source atom $\mathbf{v}_j^{(l-1)}$ and target atom $\mathbf{v}_i^{(l-1)}$:

$$\mathbf{m}_{j \rightarrow i}^{(l)} = \Phi^{(l)} \left(\mathbf{v}_j^{(l-1)}, \mathbf{e}_{ij}^{(l-1)}, \mathbf{v}_i^{(l-1)} \right) \odot \mathbf{v}_j^{(l-1)}, \forall j \in \mathcal{N}(i) \quad (2)$$

Where $\Phi^{(l)} : \mathbb{R}^d \times \mathbb{R}^d \times \mathbb{R}^d \rightarrow \mathbb{R}^d$ is the learnable message function at the l -th block, and \odot denotes element-wise multiplication. The message passing mechanism adopted here can also be viewed as an extension of continuous convolution proposed in SchNet,³⁷ with a learnable filter conditioned not only on inter-atomic distances but also interaction types between atoms, and atom properties of source and target atoms.

After all messages from neighbor atoms are collected, they are aggregated together and used to update the node embeddings.

$$\mathbf{M}_i^{(l)} = \sum_{\forall j \in \mathcal{N}(i)} \mathbf{m}_{j \rightarrow i}^{(l)} \quad (3)$$

$$\hat{\mathbf{v}}_i^{(l)} = \Theta^{(l)} \left(\mathbf{v}_i^{(l-1)}, \mathbf{M}_i^{(l)} \right) \quad (4)$$

Where $\Theta^{(l)} : \mathbb{R}^d \times \mathbb{R}^d \rightarrow \mathbb{R}^d$ is the learnable node update function at the l -th block. The node embedding input of next layer is derived by applying layer-normalization⁴² $\text{LN}(\cdot)$ and addition with residual connection.⁴³ This strategy effectively stabilizes the training of the network and enhances its overall performance.

$$\mathbf{v}_i^{(l)} = \text{LN}(\hat{\mathbf{v}}_i^{(l)}) + \mathbf{v}_i^{(l-1)} \quad (5)$$

Here we implement the message function Φ , and the node update function Θ as MLPs. Notice that, through the network, only the node embeddings are updated recursively, the edge embeddings at per-layer are derived via a learnable linear transformation from the initial encoded edge embeddings: $e_{ij}^{(l)} = \mathbf{A}^{(l)} e_{ij}^{(0)}$. In general, we find that disabling edge embedding’s recursive update will not result in performance degradation, yet it can reduce the overall computational cost significantly.

2.3 Graph Neural Force Predictor

The learnable decoder $\gamma^V : \mathbb{R}^d \rightarrow \mathbb{R}^3$ decodes high-dimensional node embeddings \mathbf{o} ($\mathbf{o}_i = \mathbf{v}_i^{(l)}, \forall i \in 1, 2, \dots, N$) at the final layer into the Cartesian forces \mathbf{f} (Figure 1, Embedding Decoding). The predicted forces are then used to update the acceleration $\ddot{\mathbf{q}}$ of each atom. The GNN-based force predictor can be flexibly integrated into any numerical integrator that has a force-based scheme. For instance, a single step in the Velocity-Verlet with GNN-based force predictor $\mathcal{F}(\cdot)$ can be written as:

$$\dot{\mathbf{q}}_{t+\Delta t/2} = \dot{\mathbf{q}}_t + \ddot{\mathbf{q}}_t \Delta t/2 \quad (6)$$

$$\mathbf{q}_{t+\Delta t} = \mathbf{q}_t + \dot{\mathbf{q}}_{t+\Delta t/2} \Delta t \quad (7)$$

$$\ddot{\mathbf{q}}_{t+\Delta t} = \mathcal{F}(\mathbf{p}, \mathbf{b}, \mathbf{q}_{t+\Delta t}) / \mathbf{m} \quad (8)$$

$$\dot{\mathbf{q}}_{t+\Delta t} = \dot{\mathbf{q}}_{t+\Delta t/2} + \ddot{\mathbf{q}}_{t+\Delta t} \Delta t/2 \quad (9)$$

where $\mathbf{p} : (\mathbf{p}_1, \dots, \mathbf{p}_N)$ denotes the atom type of every atom in the system, $\mathbf{q} : (\mathbf{q}_1, \dots, \mathbf{q}_N)$ denotes the Cartesian coordinates of every atom, and $\mathbf{b} : (\mathbf{b}_1, \dots, \mathbf{b}_k)$ denotes the edge type between every atom and their neighbor atoms.

3 Implementation Details

3.1 Software

We implement our model using PyTorch⁴⁴ (1.7.1), Deep Graph Library (0.6.0)⁴⁵ and trainer using PyTorch-Lightning (1.3.0). We generate all training data using off-the-shelf simulators from OpenMM 7.⁴⁶ We use the spatial partitioning module from JAX-MD³ to maintain the neighbor list of particles in the system.

3.2 Fixed radius graph

In GAMD, the graph is constructed via fixed radius neighbor search, where edges are established between every pairs of atoms, (i, j) , such that $\|\mathbf{q}_i - \mathbf{q}_j\|_2 < r_0$. The naive way to perform this search is by calculating the distance for every pair of particles in the system, which results in $\mathcal{O}(N^2)$ complexity. This strongly limits the scalability and efficiency of the framework. To alleviate this computational overhead, we use cell list to search for neighbors. We first partition space into different cells with size r_0 , and then for each particle we only search for neighbor among particles within the same cell and adjacent cells. Here we use `jax_md.partition.cell_list` to partition the space and `jax_md.partition.neighbor_list` to gather the neighbor list, which has an overall complexity of $\mathcal{O}(N \log N)$.

For all the systems, the cutoff radius r_0 was chosen, such that an atom has roughly 20 neighbors on average. This encompasses the range of many types of local interactions between particles, while other long-range interactions can be captured by recursive message passing in the deeper layers. In general, the choice of cutoff radius in GAMD is agnostic to the underlying interaction range of the system, which eliminates the need for selecting neighbors based on different physics rules.

3.3 Training and dataset

Dataset generation The Molecular Dynamics (MD) simulations were performed using OpenMM⁴⁶ for the ground truth molecular simulations. The systems considered in this work were uniform single atom or single molecule systems with different simulation box sizes. Periodic Boundary Conditions (PBC) were set in all directions and cut-off distance of $\sim 10\text{\AA}$ was used. Simulations are static in the initial step and pass through a transient state to reach equilibrium under constant volume and temperature (NVT), i.e. canonical, ensemble. Velocity verlet integrator along with a Nosé–Hoover chain thermostat^{47,48} with massive collisions (50/*ps*) and chain length of 10 were used to maintain the constant temperature

and consequently, kinetic energy.

Loss function The network is trained in a supervised way by minimizing the L1 distance between prediction of per-atom forces $\hat{\mathbf{f}}_i$ and ground truth \mathbf{f}_i , along with a regularization term that penalizes the total sum of the forces in the system:

$$\mathcal{L} = \frac{1}{N} \sum_{i=1}^N \|\mathbf{f}_i - \hat{\mathbf{f}}_i\| + \lambda \left\| \sum_{i=1}^N \hat{\mathbf{f}}_i \right\| \quad (10)$$

In GAMD, there is no hard-coded mechanism to restrict the range of messages a node can receive, and a node in the graph can receive messages from very distant nodes via recursive message passing. The sum of messages of a node in the final layer is essentially the high-dimensional embedding of the per-particle forces. Therefore, when the embedding contains redundant far-away messages, the final force prediction will also be influenced by unnecessary long-range interaction. To encourage the network to learn the minimal message-passing range required for predicting force accurately, we impose L1 regularization on the sum of the per-atom forces.

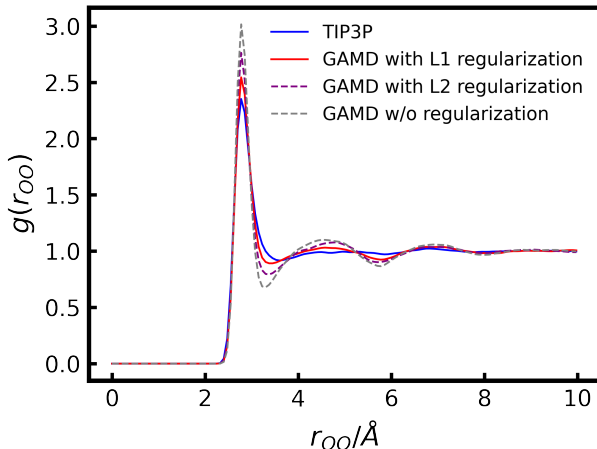


Figure 2: Comparison of model trained under different conditions. We measure the Oxygen-Oxygen RDF of water molecules’ trajectories generated from OpenMM’s TIP3P solver and GAMD models trained using: 1.L1 regularization; 2.L2 regularization; 3.Without regularization.

As shown in Figure 2, the Radial Distribution Functions (RDF) of the models trained with L2 regularization and without regularization have much sharper peaks and larger gaps compared to the ground truth, while there is a smaller gap between the RDF in the ground truth and GAMD trained under L1 regularization. This indicates that, with L1 regularization, the predicted forces agree better with ground truth and molecules are more uniformly distributed. Also it demonstrates that imposing L1 regularization can effectively suppress unnecessary long-range message passing especially when there are multiple types of interaction with different influence ranges in the system.

Training strategy For each system, we generate ten simulation trajectories with random position/velocity initialization, where we use nine trajectories as training data and validate our model on the rest one. Each sequence contains 10,000 snapshots of input, i.e. positions, and target, i.e. forces. We normalize the ground truth forces before calculating the loss, such that it has a zero mean and unit variance. We train each model for 100k iterations of gradient updates using Adam optimizer,⁴⁹ with an exponential learning rate scheduler that diminishes learning rate from $\alpha = 3 \times 10^{-4}$ to $\alpha = 1 \times 10^{-6}$. We use a batch size of 1 for all models’ training, which we found noticeably improves the performance of the models.

3.4 Benchmark setting

To compare GAMD’s performance with other classical force calculation methods, we simulate the Water box system with different sizes using GAMD, OpenMM, and LAMMPS. As GAMD only modifies the force evaluation part of every step in the MD simulation, we exclude the running time of other calculations (e.g. chain propagation, position and velocity update) in the benchmark. All the benchmarks are run on a platform equipped with a single GTX-1080 Ti GPU and i7-8700k CPU. The benchmark results and discussion is presented in the Section 4.3. Below we provide detailed configurations of benchmark for each package.

GAMD Each force calculation step of GAMD comprises two parts, building the fixed radius graph and inference. Building the graph comprises updating the neighbor list and calculating an adjacency matrix corresponding to the graph. Note that in GAMD the rebuilding of the neighbor list and graph structure is performed only when particles have traveled a distance larger than a threshold (heuristically we select this threshold as $d_r = r_{\text{cutoff}}/10$).

OpenMM To exclude the influence of other calculations involved in a single step of update, we run two simulations for each benchmark in the OpenMM. The first simulation runs in normal mode, while in the second simulation we remove all the forces defined in the system and run a dummy simulation with no forces being calculated. Then we estimate the time used to calculate forces in every step by: $t = t_0 - t_{\text{dummy}}$, where t_0 denotes the time a normal simulation will take and t_{dummy} denotes the time of dummy simulation.

LAMMPS In LAMMPS, the force calculation in an update step mainly consists of four parts according to the description in the official document: *Pair*, *Bond*, *Kspace* and *Neigh*, where *Pair* denotes the evaluation of non-bonded forces, *Bond* denotes the evaluation of bonded interactions, *Kspace* denotes the evaluation of long-range interactions and *Neigh* denotes the neighbor list construction. We report the total time of *Pair*, *Bond* and *Kspace* at each step as the time used for force evaluation, and report *Neigh* as time used for searching neighbors. Visual Molecular Dynamics (VMD)⁵⁰ is used to create water box system for LAMMPS simulation.

4 Results and discussion

In this section, we present the results of GAMD on two common MD simulation systems - Lennard-Jones particles and Water box. We calculate the Radial Distribution Function (RDF) to measure the spatial distribution of particles in a system. The RDF $g(r)$ between

two types of particles A and B is defined as:

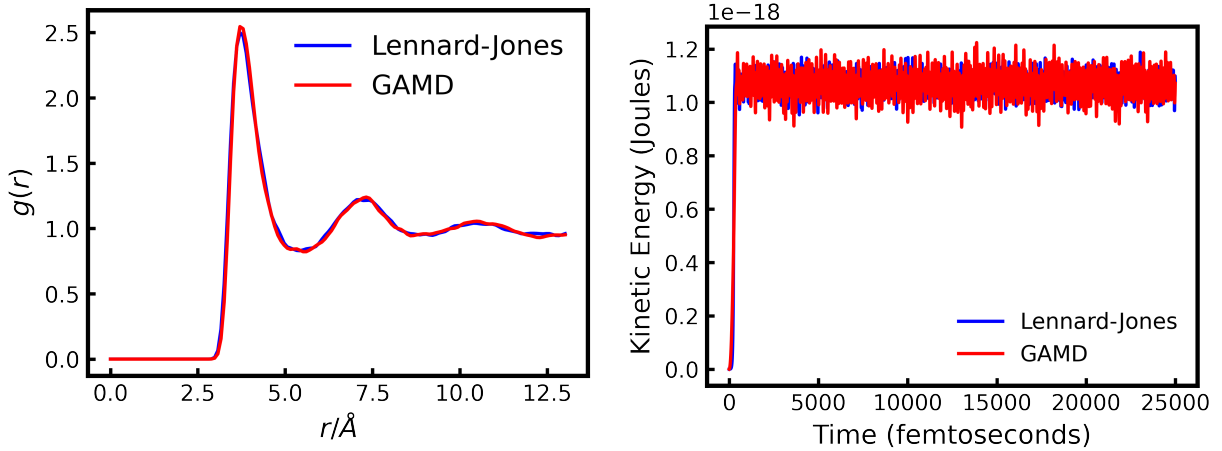
$$g(r) = \frac{1}{N_A N_B} \sum_{i=1}^{N_A} \sum_{j=1}^{N_B} \langle \delta(\|\mathbf{r}_i - \mathbf{r}_j\| - r) \rangle \quad (11)$$

where $\langle \cdot \rangle$ denotes the ensemble average, $\|\mathbf{r}_i - \mathbf{r}_j\|$ denotes the Euclidean distance between two particles i, j , r is the radius of the corresponding spherical shell, N_A and N_B denote the number of corresponding types of particles and δ filters particles' distance not falling into this shell (which we implement as a Gaussian function). Furthermore, we verify the correctness of force prediction by comparing its angle and magnitude against results from classical MD simulators.

4.1 Lennard-Jones system

We first investigate GAMD on a system consisting liquid argon with non-bonded interatomic forces governed by Lennard-Jones (LJ) potential. In this system, 258 argon atoms at 100 K are considered and the non bonded Van der Waals (VdW) potential are approximated by LJ potentials. To evaluate the performance of GAMD in the prediction of interatomic LJ forces, we first compare the RDF on argon atoms between ground truth LJ potentials and the learned model (Figure 3a). This shows how the generated trajectories keep the spatial behavior of the MD trajectories.

Since the temperature, and kinetic energy, are held constant in the NVT ensemble simulation, we can evaluate the temporal behavior of the results by comparing the kinetic energy with ground truth. Although GAMD does not have any explicit constraints for energy conservation, the trained model can successfully maintain the constant kinetic energy (Figure 3b). As mentioned before, the MD simulations are initialized from the static state with zero velocities and they reach equilibrium after a few transient steps. GAMD also has shown to be able to learn the transient state from the initial state to the equilibrium.



(a) Radial Distribution Function for particles in the Lennard-Jones system. (b) Kinetic energy trend of NVT ensemble in the Lennard-Jones system.

Figure 3: Comparison of GAMD generated trajectory with the ground truth Lennard-Jones system. The agreements in the RDF and kinetic energy indicate high precision of GAMD’s predicted forces.

The rotation-covariant predicted forces are also compared directly in terms of both direction and magnitude with the ground truth LJ forces calculated in the MD simulations. By comparing $\cos \langle \hat{\mathbf{F}}, \mathbf{F} \rangle$ between the predicted and ground truth forces, we observe that more than 95% of the predicted forces have $\cos \langle \hat{\mathbf{F}}, \mathbf{F} \rangle > 0.960$. The mean absolute error, relative error, and force direction’s accordence are reported for a sample atom number in Table 1. Also, Figure 4 illustrates this agreement between the predicted forces and the ground truth MD forces.

Table 1: Quantitative analysis of force accuracy

Atom no.	Test sample no.	$\mathcal{L}_{\text{MAE}} (eV/\text{\AA})$	$\cos \langle \hat{\mathbf{F}}, \mathbf{F} \rangle$	Relative error
258	10000	0.262	0.977	6.01%

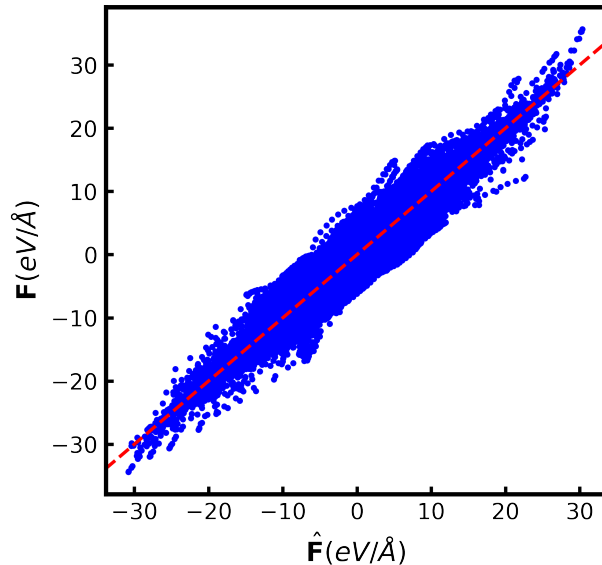


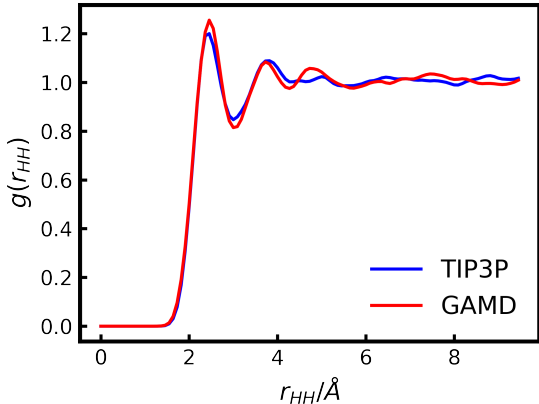
Figure 4: Ground truth forces of Lennard-Jones system with respect to the predicted forces by GAMMD. Blue dots show that predicted forces $\hat{\mathbf{F}}$ are in agreement with ground truth \mathbf{F} (red dashed line).

4.2 Water system

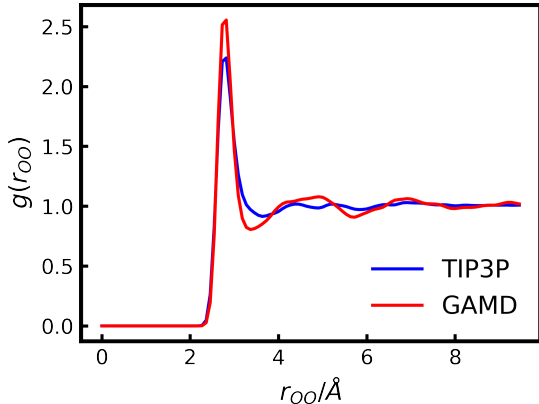
For the second experiment, we analyze GAMMD on the water box, where interactions between particles are more complex and more types of particles are involved in the dynamics. We use simulated trajectories generated by OpenMM package to train the model. The ground truth molecular simulations are performed on a box containing 258 molecules of water modeled by a three-site TIP3P water model.⁵¹ In this experiment, the model should be able to learn not only the non-bonded Van der Waals forces but also electrostatic forces due to the charges assigned to different types of atoms in a water molecule. Moreover, the model should handle two types of atoms, defined as node features, with different potentials and charges along with bonded and non-bonded interactions in and between molecules.

Similar to LJ fluid, we investigate the radial distribution function curves to evaluate the spatial behavior of the generated trajectories using GAMMD’s predicted forces. The agreement between the curves plotted for Hydrogen-Hydrogen, Oxygen-Oxygen, and Oxygen-Hydrogen element pairs shows the consistency of the GAMMD’s trajectories with the classical MD sim-

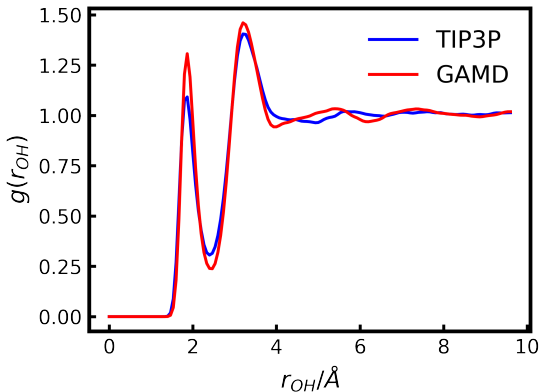
ulated trajectories (Figure 5a, 5b, 5c). Also, the transient state and equilibrium of kinetic energy is learned with high precision by GAMD and shows a similar trend with NVT MD simulation of water box (Figure 5d).



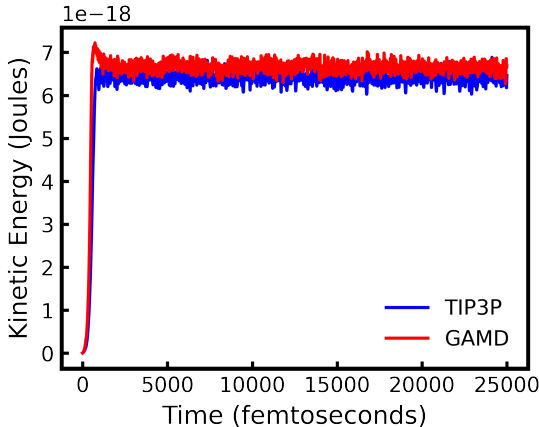
(a) RDF for Hydrogen-Hydrogen



(b) RDF for Oxygen-Oxygen



(c) RDF for Oxygen-Hydrogen



(d) Kinetic energy trend of NVT ensemble in the Water box system.

Figure 5: Comparison of GAMD generated trajectory with the ground truth water box system. The agreements in the RDF for different pairs of atoms and the kinetic energy indicate high precision of GAMD's predicted forces.

In addition to the general metrics related to the expected spatial and temporal behavior of the predicted trajectories, we can directly compare the GAMD's predicted atomic forces with the ground truth physics-based forces. Agreement in the direction of the forces is evaluated by comparing the $\cos \langle \hat{\mathbf{F}}, \mathbf{F} \rangle$ between the direction of predicted and real forces. It has been observed that in more than 95% of the predictions, $\cos \langle \hat{\mathbf{F}}, \mathbf{F} \rangle$ is of agreement

above 0.995. The relative error and mean absolute error of the predictions are reported in Table 2. Figure 6 also depicts that predicted forces in each direction are in accord with the physics-based ground truth forces.

Table 2: Quantitative analysis of force accuracy

Atom no.	Test sample no.	\mathcal{L}_{MAE} (eV/Å)	$\cos \langle \hat{\mathbf{F}}, \mathbf{F} \rangle$	Relative error
774	10000	0.9899	0.997	1.05%

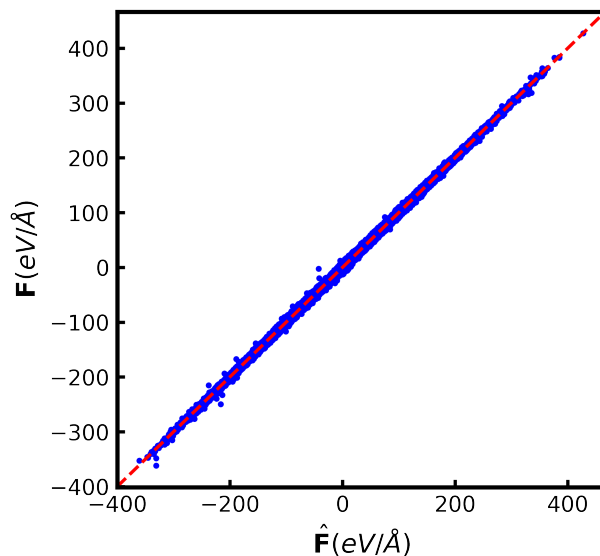


Figure 6: Ground truth forces of water box system with respect to the predicted forces by GAMM. Blue dots show that predicted forces $\hat{\mathbf{F}}$ are in agreement with ground truth \mathbf{F} (red dashed line).

4.3 Scalability and Speed

Table 3: Quantitative comparison of force calculation speed on the Water box of different scales. In GAMD and LAMMPS, the time for each force evaluation is decomposed into two parts and reported separately. *Neighbor* denotes the time needed for updating neighbor list (building graph in GNN). *Force Eval* denotes the time to evaluate the net per-atom forces based on the neighbor list. For larger system (denoted by *), OpenMM requires much smaller time step size to converge. To compare with GAMD, we report the force calculation time for OpenMM in larger systems as: $t^* = t \times \Delta t_{\langle \text{GAMD} \rangle} / \Delta t_{\langle \text{OpenMM} \rangle}$, where $\Delta t_{\langle \mathcal{S} \rangle}$ denotes the time step size used in corresponding simulator \mathcal{S} .

Molecule number	Box size (nm)	Time (ms) per force calculation step				
		OpenMM	GAMD		LAMMPS	
			Neighbor	Force Eval	Neighbor	Force Eval
258	2	0.192	2.962	4.063	0.001	0.754
887	3	0.363	3.240	4.089	0.004	3.749
2094	4	0.644	3.745	4.143	0.008	4.114
4085	5	1.310	4.445	4.035	0.010	5.431
13786	7.5	3.817	10.300	4.230	0.028	11.578
16814	8	25.454*	11.987	4.207	0.030	14.353
24093	9	31.954*	15.342	5.545	0.050	18.531

We compare our model to two high-performance MD packages, OpenMM and LAMMPS, on the Water box system under multiple scales, ranging from 2 nanometers to 9 nanometers. The major bottleneck of current GAMD’s implementation is neighbor lists’ update. The neighbor list update and graph construction in GAMD are based on JAX_MD and JAX, which are optimized for machine learning workloads and is generally slower than customized CUDA neighbor-search routines used by MD packages. This results in the noticeable gap between the time of neighbor list update in GAMD and counterparts in other MD packages. Despite this factor, GAMD still have highly competitive computing efficiency (as shown in Table 3) at the large-scale simulation which is of great importance in practical problems.⁵² Since GAMD predicts forces directly by a set of MLPs which can be efficiently parallelized on the GPU, its actual force evaluation speed is substantially faster than classical MD methods. Moreover, we believe that with a more optimized implementation of neighbor lists, GAMD’s performance can be further improved.

In general, compared to classical MD simulation methods, GAMMD offers benefits in the following aspects. First, GAMMD does not require explicit evaluation of energy and its gradient, instead, it directly predicts the net per-particle forces. Hence GAMMD can learn the forcefield directly from observed data without any prior knowledge of the underlying energy equation. Second, GAMMD does not require neighbor selection and energy accumulation based on different types of interactions (e.g. bonded interaction usually happened within a local region while non-bonded interaction happened between long-range particles). This reduces the computations needed in each step of simulation especially when there are multiple kinds of interactions in the system.

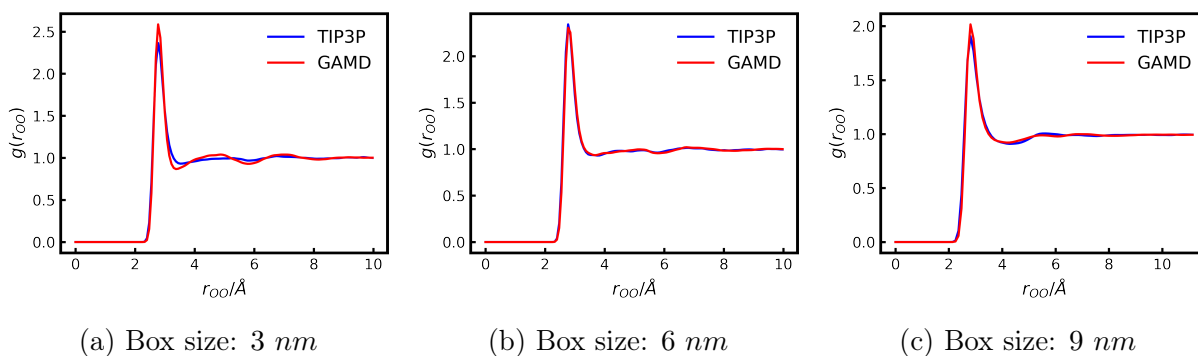


Figure 7: Radial Distribution Function for Oxygen-Oxygen distance in the Water box system of different size. (All the RDF plots are cutoff at $\sim 10\text{\AA}$)

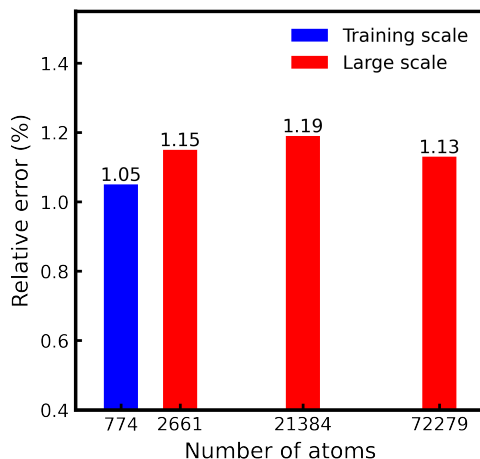


Figure 8: Relative error of force prediction on different size of water box.

Furthermore, GAMMD is a supervised machine learning model in essence, but its scalability

is not limited by the scale of training data. We find that GAMMD can learn scale-agnostic dynamics and generalize well to much larger systems. Figure 7 and Figure 8 show that GAMMD trained on a Water box with 258 water molecules can be scaled up to Water box with much more molecules (about 100 times larger) without compromising accuracy. On the largest box (Figure 7c) Water box with over 20000 molecules, GAMMD can converge under a much larger time step size (up to 5.5 femtoseconds) compared to OpenMM’s TIP3P model (up to 2.0 femtoseconds), despite GAMMD is trained on data acquired from OpenMM’s TIP3P model. This demonstrates the scalability of the model and broadens the range of the problems where GAMMD can operate.

5 Conclusion

A Graph Neural Network Accelerated Molecular Dynamics model (GAMMD) is presented. GAMMD is a GNN-based atomic force predictor which can be flexibly integrated with existing MD engines. GAMMD provides a data-driven framework that can predict atomic force directly without explicitly calculating energy. We have showcased the applications of GAMMD on two typical molecular systems - Lennard-Jones particles and Water box, where GAMMD can be used to generate MD trajectories that are consistent with existing classical MD methods in terms of spatial distribution and energy. It has also been shown that GAMMD can be scaled up to much larger systems without compromising accuracy. Furthermore, a comprehensive benchmark on GAMMD and other production-level MD engines (LAMMPS, OpenMM) is conducted which shows that despite a naive software implementation, GAMMD already has very competitive efficiency at large-scale simulation.

Acknowledgement

This work is supported by the start-up fund provided by CMU Mechanical Engineering, United States. The authors would like to thank Zhonglin Cao for valuable comments.

References

- (1) Hollingsworth, S. A.; Dror, R. O. Molecular Dynamics Simulation for All. *Neuron* **2018**, *99*, 1129–1143.
- (2) Doerr, S.; Majewski, M.; Pérez, A.; Krämer, A.; Clementi, C.; Noe, F.; Giorgino, T.; De Fabritiis, G. TorchMD: A Deep Learning Framework for Molecular Simulations. *Journal of Chemical Theory and Computation* **2021**, *17*, 2355–2363, PMID: 33729795.
- (3) Schoenholz, S. S.; Cubuk, E. D. JAX M.D. A Framework for Differentiable Physics. *Advances in Neural Information Processing Systems*. 2020.
- (4) Mailoa, J. P.; Kornbluth, M.; Batzner, S.; Samsonidze, G.; Lam, S. T.; Vandermause, J.; Ablitt, C.; Molinari, N.; Kozinsky, B. A fast neural network approach for direct covariant forces prediction in complex multi-element extended systems. *Nature Machine Intelligence* **2019**, *1*, 471–479.
- (5) Park, C. W.; Kornbluth, M.; Vandermause, J.; Wolverton, C.; Kozinsky, B.; Mailoa, J. P. Accurate and scalable graph neural network force field and molecular dynamics with direct force architecture. *npj Computational Materials* **2021**, *7*, 73.
- (6) Li, Y.; Li, H.; Pickard, F. C.; Narayanan, B.; Sen, F. G.; Chan, M. K. Y.; Sankaranarayanan, S. K. R. S.; Brooks, B. R.; Roux, B. Machine Learning Force Field Parameters from Ab Initio Data. *Journal of Chemical Theory and Computation* **2017**, *13*, 4492–4503, PMID: 28800233.
- (7) Sanchez-Gonzalez, A.; Godwin, J.; Pfaff, T.; Ying, R.; Leskovec, J.; Battaglia, P. W. Learning to Simulate Complex Physics with Graph Networks. *Proceedings of the 37th International Conference on Machine Learning, ICML 2020, 13-18 July 2020, Virtual Event*. 2020; pp 8459–8468.

- (8) Bapst, V.; Keck, T.; Grabska-Barwińska, A.; Donner, C.; Cubuk, E. D.; Schoenholz, S. S.; Obika, A.; Nelson, A. W. R.; Back, T.; Hassabis, D.; Kohli, P. Unveiling the predictive power of static structure in glassy systems. *Nature Physics* **2020**, *16*, 448–454.
- (9) Battaglia, P.; Pascanu, R.; Lai, M.; Jimenez Rezende, D.; kavukcuoglu, k. Interaction Networks for Learning about Objects, Relations and Physics. *Advances in Neural Information Processing Systems*. 2016.
- (10) Botu, V.; Batra, R.; Chapman, J.; Ramprasad, R. Machine Learning Force Fields: Construction, Validation, and Outlook. *The Journal of Physical Chemistry C* **2017**, *121*, 511–522.
- (11) Unke, O. T.; Chmiela, S.; Sauceda, H. E.; Gastegger, M.; Poltavsky, I.; Schütt, K. T.; Tkatchenko, A.; Müller, K.-R. Machine Learning Force Fields. 2021.
- (12) Wang, J.; Olsson, S.; Wehmeyer, C.; Pérez, A.; Charron, N. E.; de Fabritiis, G.; Noé, F.; Clementi, C. Machine Learning of Coarse-Grained Molecular Dynamics Force Fields. *ACS Central Science* **2019**, *5*, 755–767.
- (13) Husic, B. E.; Charron, N. E.; Lemm, D.; Wang, J.; Pérez, A.; Majewski, M.; Krämer, A.; Chen, Y.; Olsson, S.; de Fabritiis, G.; Noé, F.; Clementi, C. Coarse graining molecular dynamics with graph neural networks. *The Journal of Chemical Physics* **2020**, *153*, 194101.
- (14) Noé, F.; Tkatchenko, A.; Müller, K.-R.; Clementi, C. Machine Learning for Molecular Simulation. *Annual Review of Physical Chemistry* **2020**, *71*, 361–390, PMID: 32092281.
- (15) Gkeka, P.; Stoltz, G.; Barati Farimani, A.; Belkacemi, Z.; Ceriotti, M.; Chodera, J. D.; Dinner, A. R.; Ferguson, A. L.; Maillet, J.-B.; Minoux, H.; Peter, C.; Pietrucci, F.; Silveira, A.; Tkatchenko, A.; Trstanova, Z.; Wiewiora, R.; Lelièvre, T. Machine Learning Force Fields and Coarse-Grained Variables in Molecular Dynamics: Application to

- Materials and Biological Systems. *Journal of Chemical Theory and Computation* **2020**, *16*, 4757–4775, PMID: 32559068.
- (16) Deringer, V. L.; Caro, M. A.; Csányi, G. Machine Learning Interatomic Potentials as Emerging Tools for Materials Science. *Advanced Materials* **2019**, *31*, 1902765.
- (17) Bartók, A. P.; De, S.; Poelking, C.; Bernstein, N.; Kermode, J. R.; Csányi, G.; Ceriotti, M. Machine learning unifies the modeling of materials and molecules. *Science Advances* **2017**, *3*.
- (18) Behler, J. Atom-centered symmetry functions for constructing high-dimensional neural network potentials. *The Journal of Chemical Physics* **2011**, *134*, 074106.
- (19) Behler, J.; Parrinello, M. Generalized Neural-Network Representation of High-Dimensional Potential-Energy Surfaces. *Phys. Rev. Lett.* **2007**, *98*, 146401.
- (20) Behler, J. First Principles Neural Network Potentials for Reactive Simulations of Large Molecular and Condensed Systems. *Angewandte Chemie International Edition* **2017**, *56*, 12828–12840.
- (21) Pfaff, T.; Fortunato, M.; Sanchez-Gonzalez, A.; Battaglia, P. Learning Mesh-Based Simulation with Graph Networks. International Conference on Learning Representations. 2021.
- (22) Shlomi, J.; Battaglia, P.; Vlimant, J.-R. Graph neural networks in particle physics. *Machine Learning: Science and Technology* **2021**, *2*, 021001.
- (23) Li, Z.; Farimani, A. B. Accelerating Lagrangian Fluid Simulation with Graph Neural Networks. 2021; <https://simdl.github.io/files/34.pdf>.
- (24) Ogoke, F.; Meidani, K.; Hashemi, A.; Farimani, A. B. Graph Convolutional Neural Networks for Body Force Prediction. 2020.

- (25) Duvenaud, D. K.; Maclaurin, D.; Iparraguirre, J.; Bombarell, R.; Hirzel, T.; Aspuru-Guzik, A.; Adams, R. P. Convolutional Networks on Graphs for Learning Molecular Fingerprints. *Advances in Neural Information Processing Systems*. 2015.
- (26) Xie, T.; Grossman, J. C. Crystal Graph Convolutional Neural Networks for an Accurate and Interpretable Prediction of Material Properties. *Phys. Rev. Lett.* **2018**, *120*, 145301.
- (27) Karamad, M.; Magar, R.; Shi, Y.; Siahrostami, S.; Gates, I. D.; Barati Farimani, A. Orbital graph convolutional neural network for material property prediction. *Phys. Rev. Materials* **2020**, *4*, 093801.
- (28) Wang, Y.; Wang, J.; Cao, Z.; Farimani, A. B. MolCLR: Molecular Contrastive Learning of Representations via Graph Neural Networks. 2021.
- (29) Gilmer, J.; Schoenholz, S. S.; Riley, P. F.; Vinyals, O.; Dahl, G. E. Neural Message Passing for Quantum Chemistry. *Proceedings of the 34th International Conference on Machine Learning*. 2017; pp 1263–1272.
- (30) Chmiela, S.; Tkatchenko, A.; Sauceda, H. E.; Poltavsky, I.; Schütt, K. T.; Müller, K.-R. Machine learning of accurate energy-conserving molecular force fields. *Science Advances* **2017**, *3*.
- (31) Kearnes, S.; McCloskey, K.; Berndl, M.; Pande, V.; Riley, P. Molecular graph convolutions: moving beyond fingerprints. *Journal of Computer-Aided Molecular Design* **2016**, *30*, 595–608.
- (32) Unke, O. T.; Meuwly, M. PhysNet: A Neural Network for Predicting Energies, Forces, Dipole Moments, and Partial Charges. *Journal of Chemical Theory and Computation* **2019**, *15*, 3678–3693, PMID: 31042390.
- (33) Greydanus, S.; Dzamba, M.; Yosinski, J. Hamiltonian Neural Networks. *Advances in Neural Information Processing Systems*. 2019.

- (34) Schütt, K. T.; Arbabzadah, F.; Chmiela, S.; Müller, K. R.; Tkatchenko, A. Quantum-chemical insights from deep tensor neural networks. *Nature Communications* **2017**, *8*, 13890.
- (35) Wang, W.; Axelrod, S.; Gómez-Bombarelli, R. Differentiable Molecular Simulations for Control and Learning. ICLR 2020 Workshop on Integration of Deep Neural Models and Differential Equations. 2020.
- (36) Chmiela, S.; Sauceda, H. E.; Müller, K.-R.; Tkatchenko, A. Towards exact molecular dynamics simulations with machine-learned force fields. *Nature Communications* **2018**, *9*, 3887.
- (37) Schütt, K. T.; Kindermans, P.-J.; Sauceda, H. E.; Chmiela, S.; Tkatchenko, A.; Müller, K.-R. SchNet: A continuous-filter convolutional neural network for modeling quantum interactions. 2017.
- (38) Klicpera, J.; Groß, J.; Günnemann, S. Directional Message Passing for Molecular Graphs. International Conference on Learning Representations. 2020.
- (39) Klicpera, J.; Giri, S.; Margraf, J. T.; Günnemann, S. Fast and Uncertainty-Aware Directional Message Passing for Non-Equilibrium Molecules. *ArXiv* **2020**, *abs/2011.14115*.
- (40) Schütt, K. T.; Kessel, P.; Gastegger, M.; Nicoli, K. A.; Tkatchenko, A.; Müller, K.-R. SchNetPack: A Deep Learning Toolbox For Atomistic Systems. *Journal of Chemical Theory and Computation* **2019**, *15*, 448–455.
- (41) Hu, W.; Shuaibi, M.; Das, A.; Goyal, S.; Sriram, A.; Leskovec, J.; Parikh, D.; Zitnick, C. L. ForceNet: A Graph Neural Network for Large-Scale Quantum Calculations. 2021.
- (42) Ba, J. L.; Kiros, J. R.; Hinton, G. E. Layer Normalization. 2016.

- (43) He, K.; Zhang, X.; Ren, S.; Sun, J. Deep Residual Learning for Image Recognition. 2015.
- (44) Paszke, A.; Gross, S.; Massa, F.; Lerer, A.; Bradbury, J.; Chanan, G.; Killeen, T.; Lin, Z.; Gimelshein, N.; Antiga, L.; Desmaison, A.; Kopf, A.; Yang, E.; DeVito, Z.; Raison, M.; Tejani, A.; Chilamkurthy, S.; Steiner, B.; Fang, L.; Bai, J.; Chintala, S. In *Advances in Neural Information Processing Systems 32*; Wallach, H., Larochelle, H., Beygelzimer, A., d'Alché-Buc, F., Fox, E., Garnett, R., Eds.; Curran Associates, Inc., 2019; pp 8024–8035.
- (45) Wang, M.; Zheng, D.; Ye, Z.; Gan, Q.; Li, M.; Song, X.; Zhou, J.; Ma, C.; Yu, L.; Gai, Y.; Xiao, T.; He, T.; Karypis, G.; Li, J.; Zhang, Z. Deep Graph Library: A Graph-Centric, Highly-Performant Package for Graph Neural Networks. *arXiv preprint arXiv:1909.01315* **2019**,
- (46) Eastman, P.; Swails, J.; Chodera, J. D.; McGibbon, R. T.; Zhao, Y.; Beauchamp, K. A.; Wang, L.-P.; Simmonett, A. C.; Harrigan, M. P.; Stern, C. D.; Wiewiora, R. P.; Brooks, B. R.; Pande, V. S. OpenMM 7: Rapid development of high performance algorithms for molecular dynamics. *PLoS Computational Biology* **2017**, *13*, 1–17.
- (47) Nosé, S. A unified formulation of the constant temperature molecular dynamics methods. *The Journal of Chemical Physics* **1984**, *81*, 511–519.
- (48) Hoover, W. G. Canonical dynamics: Equilibrium phase-space distributions. *Phys. Rev. A* **1985**, *31*, 1695–1697.
- (49) Kingma, D. P.; Ba, J. Adam: A Method for Stochastic Optimization. 2017.
- (50) Humphrey, W.; Dalke, A.; Schulten, K. VMD: Visual molecular dynamics. *Journal of Molecular Graphics* **1996**, *14*, 33 – 38.

- (51) Jorgensen, W. L.; Chandrasekhar, J.; Madura, J. D.; Impey, R. W.; Klein, M. L. Comparison of simple potential functions for simulating liquid water. *The Journal of Chemical Physics* **1983**, *79*, 926–935.
- (52) Zhao, G.; Perilla, J.; Yufenyuy, E.; Meng, X.; Chen, B.; Ning, J.; Ahn, J.; Gronenborn, A.; Schulten, K.; Aiken, C.; Zhang, P. Mature HIV–1 Capsid Structure by Cryo–Electron Microscopy and All–Atom Molecular Dynamics. *Nature* **2013**, *497*, 643–646.